Separation and Purification Technology 179 (2017) 184–193

Contents lists available at ScienceDirect

Separation and Purification Technology

journal homepage: www.elsevier.com/locate/seppur

Magnetically recyclable Fe_3O_4/Bi_2S_3 microspheres for effective removal of Congo red dye by simultaneous adsorption and photocatalytic regeneration

Huayue Zhu [a,b,c], Ru Jiang [a,b,c,*], Jianbing Li [b,**], Yongqian Fu [a], Shengtao Jiang [a,c], Jun Yao [a,c]

[a] Zhejiang Provincial Key Laboratory of Plant Evolutionary Ecology and Conservation, Taizhou University, Taizhou, Zhejiang 318000, China
[b] Environmental Engineering Program, University of Northern British Columbia, Prince George, British Columbia V2N 4Z9, Canada
[c] Department of Environmental Engineering, Taizhou University, Taizhou, Zhejiang 318000, China

ARTICLE INFO

Article history:
Received 17 June 2016
Received in revised form 6 December 2016
Accepted 21 December 2016
Available online 7 January 2017

Keywords:
Bismuth sulfide
Magnetic material
Photocatalysis
Adsorption
Congo red

ABSTRACT

Novel magnetic bayberry-like Fe_3O_4/Bi_2S_3 microspheres (Fe_3O_4/Bi_2S_3 MSs) combining highly effective adsorption and photocatalytic regeneration were prepared by a facile hydrothermal method. The resultant Fe_3O_4/Bi_2S_3 MSs were characterized by XRD, SEM, EDS, VSM, BET and DRS. Fe_3O_4/Bi_2S_3 MSs possessed a relative large surface area of 36.0 $m^2\ g^{-1}$ and narrow pore size distribution around 4.72 nm. The equilibrium and kinetics of adsorption process followed the Langmuir isotherm model and pseudo-second-order kinetic model, respectively. Maximum adsorption capacity of CR as 92.24 mg g^{-1} was achieved on Fe_3O_4/Bi_2S_3 MSs, while only 66.28 mg g^{-1} was found on Bi_2S_3 MSs. High saturation magnetization, low coercivity and remnant magnetization values of Fe_3O_4/Bi_2S_3 MSs indicated that easy separation and fast re-dispersion in aqueous solution can be realized. What's more important, Fe_3O_4/Bi_2S_3 MSs with a stronger absorption in the visible light region can be regenerated by photocatalysis under simulated solar light irradiation. Fe_3O_4/Bi_2S_3 MSs also showed excellent stability and reusability for continuous removal of Congo red dye by synergistic adsorption and photocatalytic regeneration. As a result, Fe_3O_4/Bi_2S_3 MSs provided effective and conveniently recyclable materials for environmental remediation by means of providing the facile preparation, easy magnetic separation, high adsorption, and simple regeneration.

1. Introduction

According to the Colour Index, over 10,000 types of dyes are being manufactured, and annual worldwide dye production is more than 700,000 tons. It is estimated that about 10% of dyes used in industry are finally discharged into the aqueous environment, which is quite harmful to the human health and aquatic ecosystem due to their high carcinogenicity and toxicity [1]. For effective removal of those dyes from industrial wastewater, various techniques, including adsorption [2,3], flocculation-coagulation [4], ozonation [5], sonocatalysis [6], and photocatalysis [7–9], have been developed recently. Among those approaches, synergistic method of adsorption and photocatalysis has been shown to be an effective method to treat containing-dye wastewater [8–13].

As a direct band gap material with a gap energy (Eg) of 1.3 eV, bismuth sulfide (Bi_2S_3) has drawn intensive attention for its potential applications in photocatalysis [14–16], electrochemical applications [17–19], photodetector [20,21], environmental remediation [22–24], and solar energy conversion [25,26]. Recently, many Bi_2S_3-based nanocomposites, such as SiO_2/Bi_2S_3 [27], $BiVO_4/Bi_2S_3$ [14], Bi_2S_3/In_2S_3 [28], Bi_2S_3-BiOCl [29], CuS/Bi_2S_3 [30], Bi_2S_3/Bi_2SiO_5 [31], $Bi_2S_3/g\text{-}C_3N_4$ [22], and Bi_2S_3/Bi_2WO_6 [16], have been successfully fabricated by different techniques, and their novel and unique adsorption and photocatalytic properties have been extensively explored. Those studies have demonstrated that Bi_2S_3-based nanocomposites possess excellent photocatalytic performance for eliminating various toxic organic pollutants [22,23,27,28]. However, because of their small sizes, easy recovery and continuous reusility of Bi_2S_3-based nanocomposites are still a challenge in practical treatment system.

The separation and recovery of nanomaterials from solution with the use of magnetic fields is more selective, efficient and faster than centrifugation or filtration [32]. Magnetically recyclable

* Corresponding author at: No. 1139, Municipal Government Avenue, Taizhou City, Zhejiang Province 318000, China.
** Corresponding author.
E-mail addresses: jiangru0576@163.com (R. Jiang), Jianbing.Li@unbc.ca (J. Li).

http://dx.doi.org/10.1016/j.seppur.2016.12.051
1383-5866/

materials has become an active and important field of corresponding researches [33–35]. Some magnetic chemicals have been used as the magnetic carriers, such as Fe_3O_4 [32,36–38], γ-Fe_2O_3 [9,35] and MFe_2O_4 (M = Ni, Co, Zn, Cu) [13,39], to prepare all kinds of magnetic nanocomposites. Among them, Fe_3O_4 nanoparticles with good magnetic response can accomplish the simple magnetic separation and recovery of suspended nanocomposites using an external magnet [37,40,41]. In addition, the excellent adsorption ability of Fe_3O

3. Results and discussion

3.1. Characterization of materials

3.1.1. XRD analysis and UV–vis diffuse reflectance spectra

Fig. 1a represents XRD patterns of pure Fe_3O_4, Bi_2S_3 MSs and Fe_3O_4/Bi_2S_3 MSs. It can be easily found that the diffraction peaks of pure Fe_3O_4 at $2\theta = 30.32°$, 35.64°, 43.36°, 53.66°, 57.26° and 62.87° match the reflections of (220), (311), (400), (422), (511) and (440), respectively, indexed to the cubic spinel structure of Fe_3O_4 (JCPDS 56-3107) (Fig. 1a) [44]. All of the diffraction peaks of Bi_2S_3 MSs are in good accordance with the standard card of orthorhombic Bi_2S_3 (JCPDS 75-1306) [17]. The pattern of Fe_3O_4/Bi_2S_3 MSs exhibit a coexistence of the Fe_3O_4 and Bi_2S_3, indicating the formation of the nanocomposites. No additional phases are evident found from the XRD patterns of all samples. The crystalline sizes of Fe_3O_4 and Bi_2S_3, determined by the Debye–Scherrer equation [40], were found to be 9 and 4 nm, respectively. Yavuz's research showed that 8–12 nm–size represents the optimal size for magnetic separations [32], which is further demonstrated below by VSM studies.

Fig. 1b displays the UV–vis diffuse reflectance spectra (DRS) of Fe_3O_4, Bi_2S_3 MSs and Fe_3O_4/Bi_2S_3 MSs. It is worth noting that Bi_2S_3 MSs have strong absorption over the whole visible light region [14,29]. The band gap of pure Bi_2S_3 is about 1.3 eV [22]. Pure Fe_3O_4 has photo-absorption not only in UV light range, but also in visible light range. However, light absorption of Fe_3O_4 weakens with increasing wavelength in the range of visible light. The whole light absorption ability of the Fe_3O_4/Bi_2S_3 MSs increased obviously with the introduction of Bi_2S_3, which should be attributed to the small band gap and large absorption coefficient of Bi_2S_3 [49]. Compared with the magnetic photocatalysts reported in literatures [29,43,44], Fe_3O_4/Bi_2S_3 MSs have strong absorption in the UV–visible-light region from 200 to 800 nm, implying it possible to regenerate the materials by photocatalysis under simulated solar light irradiation after Fe_3O_4/Bi_2S_3 MSs have adsorbed targeted pollutants.

3.1.2. Morphology and microstructure

The surface morphology, microstructure and sizes of Bi_2S_3 [illegible] and Fe_3O_4/Bi_2S_3 MSs were determined by SEM. Fig. 2a sho[illegible] low-magnification SEM image of Bi_2S_3 MSs by hydro[illegible] method using thiocarbamide as sulfur source. It reveals[illegible] MSs consisted of bayberry-like microspheres with [illegible] in the range of 1.3–4.5 [illegible] Bi_2S_3 MSs shows th[illegible] structed with nanor[illegible] the center of the mi[illegible] archical bayberry-li[illegible] tion of ferroferric o[illegible] Bi_2S_3 MSs with ar[illegible] obtained (Fig. 2c), a[illegible] and Fe_3O_4 nanopa[illegible] Fe_3O_4/Bi_2S_3 MSs [illegible] are more uneven [illegible] the presence of [illegible] Bi_2S_3 crystal to s[illegible] tions on Fe_3O_4[illegible] dispersive spect[illegible] analysis of the [illegible] and O, which [illegible] nanorods. How[illegible] the microsphe[illegible] of Fe_3O_4/Bi_2S_3[illegible]

3.1.3. Vibratin[illegible]

The magn[illegible] MSs were m[illegible] Fig. 3. The [illegible] was 66.50 [illegible] the literatu[illegible] Fe_3O_4/Bi_2S_3[illegible] of bismuth[illegible] reported [illegible] Fe_3O_4/ZnO[illegible] indicated[illegible] magne[illegible] plet[illegible] by[illegible]

.6[illegible]

e3O[illegible]

lting [illegible] of as-

prepar[illegible] ent magnet was

remov[illegible] ly re-dispersed in aque-

ous s[illegible] of ultrasound, demonstrating that

easy, [illegible] d redispersion of the Fe_3O_4/Bi_2S_3 MSs can

be re[illegible] aqueous solution. Combined with the other unique

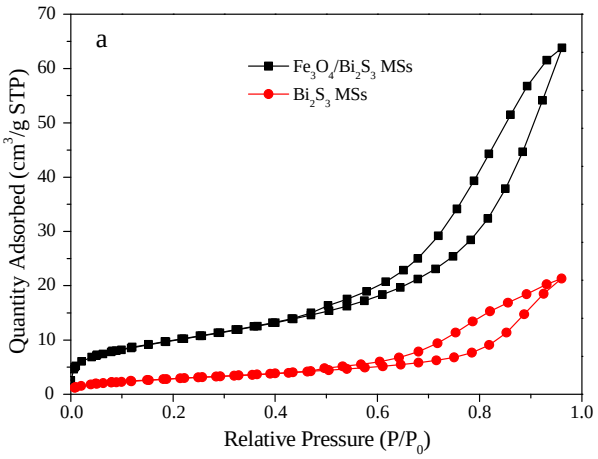

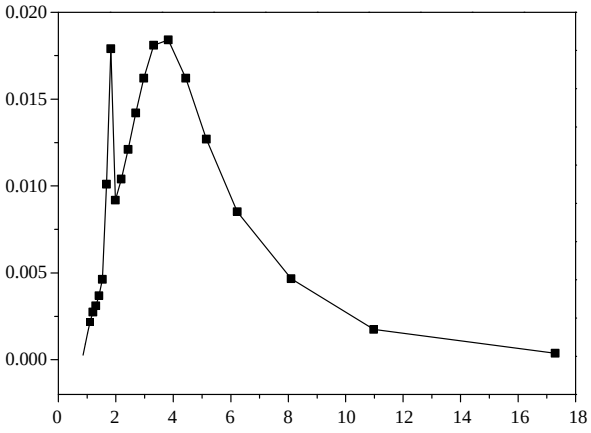

3.2. Adsorption isotherms

Adsorption isotherm is one of important data to explain the adsorption mechanism of contaminant on novel nanocomposite [27]. In addition, the adsorption of dye on nanocomposites is an important prerequisite for a synergistic adsorption-photocatalytic degradation process [8]. Therefore, Langmuir and Freundlich isotherm models were used to analyze the equilibrium adsorption characteristics for CR dye on Bi_2S_3 MSs and Fe_3O_4/Bi_2S_3 MSs. Langmuir and Freundlich equations is represented for Eqs. (3) and (4), respectively [3].

$$\frac{c_e}{q_e} = \frac{1}{bq_m} + \frac{c_e}{q_m} \tag{3}$$

$$\ln q_e = \ln K_F + \frac{1}{n} \ln c_e \tag{4}$$

where c_e (mg L^{-1}) is equilibrium concentration of CR in solution, q_e (mg g^{-1}) is the adsorption capacity of CR adsorbed at equilibrium, q_m (mg g^{-1}) is maximum amounts of CR adsorbed per unit mass of adsorbent required for monolayer coverage of the surface, b (L mg^{-1}) is a constant related to the heat of adsorption. The slope and intercept of linear plots of c_e/q_e against c_e yield the values of $1/q_m$ and $1/bq_m$ for Eq. (3). K_F ($mg^{1-(1/n)}$ $L^{1/n}$ g^{-1}) is related to the adsorption capacity of the adsorbent and $1/n$ is another constant related to the surface heterogeneity. The slope and intercept of linear plots of $\ln q_e$ against $\ln c_e$ yield the values of $1/n$ and $\ln K_F$ for Eq. (4).

Fig. 5 shows the isotherms of CR adsorption on Bi_2S_3 MSs and Fe_3O_4/Bi_2S_3 MSs, while their maximum adsorption capacities (q_m) and some theoretical parameters (q_m, b, K_F, n, and R^2) are summarized in Table 1. It was notable that an increase in temperature resulted in a corresponding increase in adsorption capacity of CR on both Bi_2S_3 MSs and Fe_3O_4/Bi_2S_3 MSs, which showed that the adsorptions of CR onto Bi_2S_3 MSs and Fe_3O_4/Bi_2S_3 MSs are endothermic process. In general, the Langmuir isotherm model describes monolayer adsorption process while the Freundlich isotherm model describes the adsorption on heterogeneous surfaces associated with several adsorbent–adsorbate interactions [27]. For the CR adsorption on Bi_2S_3 MSs, the R^2 values ($R^2 > 0.968$) from the Freundlich equation (Eq. (4)) were all higher than those ($R^2 < 0.890$) from the Langmuir model (Eq. (3)), which is responsible for the observed multilayer adsorption. However, for the CR adsorption on Fe_3O_4/Bi_2S_3 MSs, the Langmuir equation represented the adsorption process and all R^2 values were higher than 0.972, indicating that monolayer coverage of the dye adsorbed on the surface of Fe_3O_4/Bi_2S_3 MSs. With the introduction of Fe_3O_4, magnetic Fe_3O_4/Bi_2S_3 MSs have bayberry-like structures, rough and porous surfaces and exposed more adsorption sites. As a result, the adsorption of CR on Fe_3O_4/Bi_2S_3 MSs presents monolayer adsorption process. This result is in good agreement with the observations in SEM and BET analysis of Bi_2S_3 MSs and Fe_3O_4/Bi_2S_3 MSs.

Table 2 compares the adsorption capacity of the magnetic Fe_3O_4/Bi_2S_3 MSs with the other reported inorganic adsorbents. The maximum adsorption capacity of the magnetic Fe_3O_4/Bi_2S_3 MSs towards CR is 92.24 mg g^{-1}, which is higher than those of adsorbents reported earlier, such as $Fe_{3-x}La_xO_4$ ferrite [53], Zn-Fe_2O_4 [54], Ca-bentonite [55], chitosan coated magnetic Fe_3O_4 particle [56], activated carbon [57]. It is worth mentioning that the maximum adsorption capacity (92.24 mg g^{-1}) of CR on Fe_3O_4/Bi_2S_3 MSs was almost 12.76 times higher than that of the reported activated carbon (6.7 mg g^{-1}) [57]. Therefore, Fe_3O_4/Bi_2S_3 MSs are suitable and promising for CR removal from aqueous solutions since it has a relatively high adsorption capacity and easy magnetic separation.

3.3. Effect of initial CR concentration on adsorption

Fig. 6 presents the time-dependent adsorption performance of the Bi_2S_3 MSs and magnetic Fe_3O_4/Bi_2S_3 MSs towards the removal of CR at different initial dye concentrations in aqueous solutions.

Table 2
The q_m values for the adsorption of CR on different adsorbents.

Adsorbents	q_m (mg g^{-1})	Ref.
Fe_3O_4/Bi_2S_3 MSs	92.24	This study
Chitosan coated magnetic Fe_3O_4 particle	42.62–56.66	[56]
$Fe_{3-x}La_xO_4$ ferrite	37.4–79.1	[53]
Zn-Fe_2O_4	16.58	[54]
Ca-bentonite	23.25–85.29	[55]
Activated carbon	6.7	[57]

For Bi_2S_3 MSs, as the initial concentration increased from 5 mg L^{-1} to 30 mg L^{-1}, the removal rate of CR decreased from 99% to 60% (Fig. 6a). However, the percentage of CR adsorption on Fe_3O_4/Bi_2S_3 MSs reached up to 85% within 90 min for all the studied concentrations (Fig. 6b). Compared with CR adsorption process on Bi_2S_3 MSs, the fast adsorption over the magnetic Fe_3O_4/Bi_2S_3 MSs was clearly observed for all the studied concentrations. This higher efficiency and faster rate of CR adsorption on Fe_3O_4/Bi_2S_3 MSs can be ascribed to abundant unoccupied active sites on the adsorbent's surface as well as the porous hierarchical structure of the magnetic Fe_3O_4/Bi_2S_3 MSs [3]. On the basis of the above results, the observed high adsorption capacity and the short time needed to achieve adsorption equilibrium confirm the magnetic Fe_3O_4/Bi_2S_3 MSs would be an effective adsorbent for CR removal.

3.4. Adsorption kinetics

Adsorption kinetics is one of the most important characters which govern the solute uptake rate and represent adsorption efficiency of adsorbent for design operation and optimization. To investigate adsorption kinetics of CR on Bi_2S_3 MSs and magnetic Fe_3O_4/Bi_2S_3 MSs, three different kinetic models, i.e. Lagergren-first-order model, pseudo-second-order kinetic model and intraparticle diffusion model were used to fit the adsorption kinetic data.

The Lagergren-first-order kinetic, pseudo-second-order kinetic model and intraparticle diffusion model can be given by Eqs. (5)–(7) [55].

$$\log\,(q_e - q_t) = \log\, q_e - \frac{k_1 t}{2.303} \tag{5}$$

$$\frac{t}{q_t} = \frac{1}{k_2 q_e^2} + \frac{1}{q_e} t \tag{6}$$

$$q_t = k_{id} t^{1/2} + c \tag{7}$$

where q_e and q_t (mg g^{-1}) are the amounts of CR adsorbed at equilibrium and at time t (min), respectively; k_1 is the rate constant of Lagergren-first-order kinetic model (min^{-1}). Values of k_1 can be calculated from the plots of $\log(q_e - q_t)$ versus t for Eq.(5). k_2 is the rate constant (g mg^{-1} min^{-1}) of pseudo-second-order kinetic model for adsorption. The slope and intercept of the linear plots of t/q_t against

Table 1
Adsorption isotherm constants for CR adsorption onto Bi_2S_3 MSs and magnetic Fe_3O_4/Bi_2S_3 MSs.

Adsorbent	T (°C)	$q_{e,exp}$ (mg g^{-1})	Langmuir isotherm constants			Freundlich isotherm constants		
			q_m (mg g^{-1})	b	R^2	K_F ($mg^{1-(1/n)}$ $L^{1/n}$ g^{-1})	n	R^2
Bi_2S_3 MSs	25	37.44	33.39	0.250	0.830	15.75	6.27	0.982
	35	48.48	41.36	0.736	0.813	22.81	7.69	0.972
	45	54.62	46.86	0.826	0.861	24.45	6.98	0.968
	55	66.28	56.27	0.912	0.890	26.91	6.08	0.980
Fe_3O_4/Bi_2S_3 MSs	25	53.33	55.25	0.376	0.981	23.63	5.51	0.963
	35	72.23	70.97	0.629	0.972	28.50	4.93	0.968
	45	77.24	78.064	1.073	0.973	32.45	5.07	0.962
	55	92.24	90.580	1.302	0.987	35.72	4.79	0.958

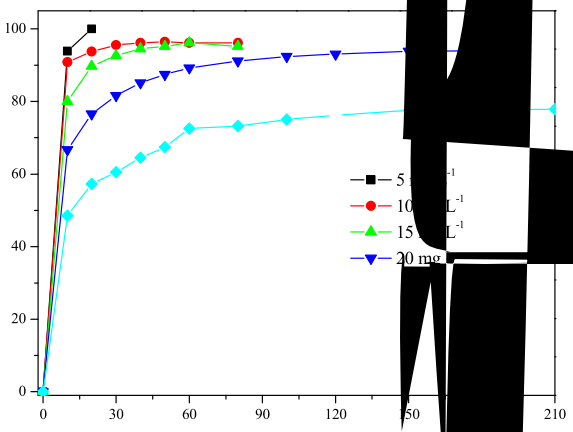

t yield the values of $1/q_e$ and $1/k_2q_e^2$ for Eq. (6). c (mg … the intercept and k_{id} is the intraparticle diffusion rate … tant (mg g^{-1} $min^{-1/2}$), which can be calculated from the slop… lin-ear plots of q_t versus $t^{1/2}$.

Different kinetic parameters of CR adsorption onto … MSs and Fe_3O_4/Bi_2S_3 MSs for different CR initial concentrati… were shown in Table 3. The relatively low correlation coeffi… (R^2) and the large difference between the calculated value of ad… otion capacity ($q_{e,cal}$) and the experimental value ($q_{e,exp}$) indicate… t the adsorption kinetics of CR on the magnetic Fe_3O_4/Bi_2S_3 MSs … s not obey the pseudo-first-order kinetic model. However, all th… xper-imental data showed better compliance with pseudo-secon… order kinetic model in terms of higher correlation coefficient values ($R^2 > 0.998$) and closer values between $q_{e,cal}$ and $q_{e,exp}$ (Table 3). It could be found that pseudo-second-order kinetic model was more valid to describe the adsorption behavior of CR onto Fe_3O_4/Bi_2S_3 MSs, indicating that the adsorption of CR on both Bi_2S_3 MSs and magnetic Fe_3O_4/Bi_2S_3 MSs are mainly controlled by chemisorption. Fig. 7 showed the regression plots of pseudo-second-order kinetic model about CR adsorption on both Bi_2S_3 MSs and magnetic Fe_3O_4/Bi_2S_3 MSs. It was likely that the adsorption behavior may involve valence forces by sharing of electrons between anions and bio-adsorbent.

3.5. Photocatalytically recycling under simulated solar light

In addition to efficiency, the lifetime of water-treatment materials is also very important for practical applications. The reuse ability can be realized if Fe_3O_4/Bi_2S_3 MSs can self-clean CR dye molecules absorbed on it. Therefore, the reutility and stability of the magnetic Fe_3O_4/Bi_2S_3 MSs were examined through the repeated experiments based on the two different experimental procedures: (1) only adsorption in dark and (2) simultaneous adsorption and photocatalytic regeneration in one step for cycling under simulated solar light irradiation. Fig. 8 shows the successive cycles of two different experimental procedures. The adsorption capacities for Fe_3O_4/Bi_2S_3 MSs decreased noticeably during the repeated adsorption operations. An obvious decrease from 91.60% to 40.3% in the removal efficiency was observed when the magnetic Fe_3O_4/Bi_2S_3 MSs were reused as adsorbent for the first cycle (Fig. 8 curve a). After the successive fifth cycles, the removal efficiency was only 25.3% by only adsorption in dark. The decreased efficiency after five cycles may be due to the decreased surface active sites. Interestingly, when the adsorption and photocatalytic regeneration were simultaneously performed during the repeated experiments under simulated solar light irradiation, the recyclability of the magnetic Fe_3O_4/Bi_2S_3 MSs can be improved efficiently compared with the reuse of Bi_2S_3 MSs. As shown in Fig. 8 curve b, the magnetic Fe_3O_4/Bi_2S_3 MSs exhibited good stability and maintained high removal efficiency in successive five cycles under simulated solar light irradiation. What's more, the magnetic Fe_3O_4/Bi_2S_3 MSs did not show a clear decrease in photodegradation efficiency after Fe_3O_4/Bi_2S_3 MSs were used for fifth time recycles for the decolorization of CR under simulated light irradiation. The enhanced decolorization of CR solution by Fe_3O_4/Bi_2S_3 MSs resulted from two main reasons. Firstly, Fe_3O_4/Bi_2S_3 MSs can concentrate the targeted CR dye on the surface of water-treatment materials from the diluted water to promote the CR transfer process. Secondly, CR adsorbed on the surface of Fe_3O_4/Bi_2S_3 MSs can be photocatalytically oxidized and the adsorbent can be regenerated and reused in further cycles [27]. Several studies have shown that CR moleculars can be photodecolorized by appropriated photocatalysts under light irradiation [9,58]. Bi_2S_3 with a typical narrow band gap can be used to photodegrade organic pollutant since Fe_3O_4/Bi_2S_3 MSs have a stronger absorption in the visible light area. In addition, the fact that adsorption and photocatalytic regeneration of organic compounds occur continuously in the presence of Fe_3O_4/Bi_2S_3 MSs avoids two independent processes and reduces the actual processing cost. As a result, magnetically recyclable Fe_3O_4/Bi_2S_3 MSs could be regenerated via the

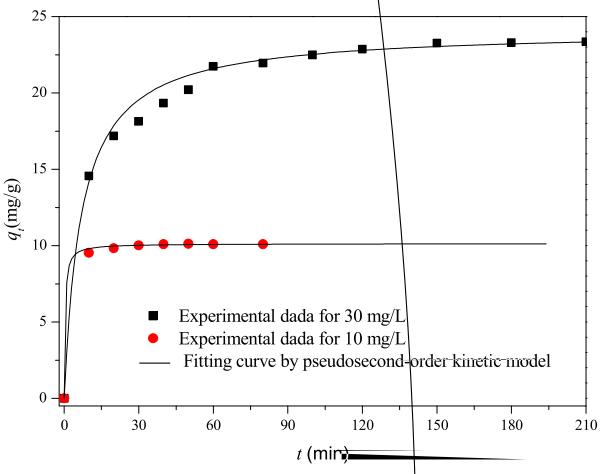

economical, green photocatalytic treatment and maintain higher processing removal efficiency of CR dye by adsorption and photocatalytic regeneration.

3.6. The possible mechanism of dye removal by Fe_3O_4/Bi_2S_3 MSs

As previous studies mentioned [29,46], the photodegradation of dye pollutants on photocatalyst is mainly driven by a series of reactive species including active holes (h^+), hydroxyl radicals ($\cdot OH$), and superoxide radicals ($O_2^{\cdot-}$) generated. Based on the above experimental results and corresponding Refs. [44,46], a possible mechanism of successful CR removal by Fe_3O_4/Bi_2S_3 MSs under simulated solar light irradiation was proposed as follows (Fig. 9). Firstly, CR molecules in aqueous solution were adsorbed fast onto Fe_3O_4/Bi_2S_3 MSs (Eq. (8)) due to the high relative large surface areas and mesoporous channels of magnetic Fe_3O_4/Bi_2S_3. At the same time, electrons (e^-) in the valence band (VB) of Bi_2S_3 in Fe_3O_4/Bi_2S_3 MSs can be photoexcited to its conduction band (CB) under simulated light irradiation, causing the photoproduced holes (h^+) in the VB of Bi_2S_3 simultaneously (Eq. (9)). The CB level of Fe_3O_4 (1 V vs. NHE) is much lower than that of Bi_2S_3 (0.12 V vs. NHE) [22,46], so the photoproduced $Bi_2S_3(e^-)$ may quickly migrate from conduction band of Bi_2S_3 MSs into that of the Fe_3O_4 and the chance of e^-/h^+ recombination is greatly reduced (Eq. (10)). Following, the migrated e^- reacted with the oxygen molecule (O_2) that dissolved in aqueous solution to yield $O_2^{\cdot-}$ (Eq. (11)) [29], which further react with H_2O and to produce H_2O_2 and $\cdot OH$ (Eqs. (12) and (13)). The photoinduced holes (h^+) at the VB top of Bi_2S_3 with potential of about 2.07 eV [31], which is more positive than the standard reduction potential of $OH^-/\cdot OH$(1.99 eV), can react with H_2O to produce $\cdot OH$ radicals (Eq. (14)). At last, all the produced active species including $\cdot OH$, e^-/h^+ and $O_2^{\cdot-}$ can attacked the N=N bonds of CR molecules adsorbed on Fe_3O_4/Bi_2S_3 MSs and further oxidize the broken CR molecules into CO_2, H_2O and other small molecule byproducts (Eq. (15)) [29].

$$CR\ (\text{in aqueous solution}) + Fe_3O_4/Bi_2S_3 \rightarrow CR - Fe_3O_4/Bi_2S_3 \quad (8)$$

$$Bi_2S_3 + h\nu \rightarrow Bi_2S_3\ (h^+ + e^-) \quad (9)$$

$$Bi_2S_3\ (h^+ + e^-) + Fe_3O_4 \rightarrow Fe_3O_4\ (e^-) + Bi_2S_3(h^+) \quad (10)$$

$$Fe_3O_4\ (e^-) + O_2 \rightarrow Fe_3O_4 + O_2^{\cdot-} \quad (11)$$

$$2O_2^{\cdot-} + 2H_2O \rightarrow 2OH^- + H_2O_2 + O_2 \quad (12)$$

$$H_2O_2 + Fe_3O_4(e^-) \rightarrow \cdot OH + OH^- + Fe_3O_4 \quad (13)$$

$$Bi_2S_3\ (h^+) + H_2O \rightarrow Bi_2S_3 + \cdot OH + H^+ \quad (14)$$

$$CR + O_2^{\cdot-}/\cdot OH/h^+ \rightarrow CO_2 + H_2O + \text{other small molecule byproducts} \quad (15)$$

4. Conclusions

In summary, magnetically recyclable Fe_3O_4/Bi_2S_3 MSs combining the highly effective adsorption and green photocatalytic regeneration were prepared by a facile hydrothermal method. The as-obtained Fe_3O_4/Bi_2S_3 MSs possessed a relative high surface area, low coercivity value and remanent magnetization value. The Fe_3O_4/Bi_2S_3 MSs can be easily and economically separated, regenerated and re-dispersed in aqueous solution, which is desirable

[39] R. Jiang, H.Y. Zhu, J.B. Li, F.Q. Fu, J. Yao, S.T. Jiang, G.M. Zeng, Fabrication of novel magnetically separable BiOBr/$CoFe_2O_4$ microspheres and its application in the efficient removal of dye from aqueous phase by an environment-friendly and economical approach, Appl. Surf. Sci. 364 (2015) 604–612.
[40] X. Li, C. Niu, D. Huang, X. Wang, X. Zhang, G. Zeng, Q. Niu, Preparation of magnetically separable Fe_3O_4/BiOI nanocomposites and its visible photocatalytic activity, Appl. Surf. Sci. 286 (2013) 40–46.
[41] Y.F. Zhang, L.G. Qiu, Y.P. Yuan, Y.J. Zhu, X. Jiang, J.D. Xiao, Magnetic Fe_3O_4@C/Cu and Fe_3O_4@CuO core–shell composites constructed from MOF–based materials and their photocatalytic properties under visible light, Appl. Catal., B 144 (2014) 863–869.
[42] M. Farrokhi, S.C. Hosseini, J.K. Yang, M. Shirzad-Siboni, Application of ZnO–Fe_3O_4 nanocomposite on the removal of azo dye from aqueous solutions: kinetics and equilibrium studies, Water Air Soil Pollut. 225 (2014) 2113–2124.
[43] Y.R. Yao, W.Z. Huang, H. Zhou, H.Y. Yin, Y.F. Zheng, X.C. Song, A novel Fe_3O_4@SiO_2@BiOBr photocatalyst with highly active visible light photocatalytic properties, Mater. Chem. Phys. 148 (2014) 896–902.
[44] C. Karunakaran, P. Vinayagamoorthy, J. Jayabharath, Nonquenching of charge carriers by Fe_3O_4 core in Fe_3O_4/ZnO nanosheet photocatalyst, Langmuir 30 (2014) 15031–15039.
[45] X. Bian, K. Hong, X. Ge, R. Song, L. Liu, M. Xu, Functional hierarchical nanocomposites based on ZnO nanowire and magnetic nanoparticle as highly active recyclable photocatalysts, J. Phys. Chem. C119 (2015) 1700–1705.
[46] Y. Cao, C. Li, J. Li, Q. Li, J. Yang, Magnetically separable Fe_3O_4/AgBr hybrid materials: highly efficient photocatalytic activity and good stability, Nanoscale Res. Lett. 10 (2015) 251–256.
[47]